Photon-phonon entanglement in coupled optomechanical arrays

Uzma Akram,[1,*] William Munro,[2,3] Kae Nemoto,[3] and G. J. Milburn[1]

[1]*Centre for Engineered Quantum Systems, School of Mathematics and Physics, The University of Queensland, St Lucia, QLD 4072, Australia*
[2]*NTT Basic Research Laboratories, NTT Corporation, 3-1 Morinosato-Wakamiya, Atsugi, Kanagawa 243-0198, Japan*
[3]*National Institute of Informatics, 2-1-2 Hitotsubashi, Chiyoda-ku, Tokyo 101-8430, Japan*

We consider an array of three optomechanical cavities coupled either reversibly or irreversibly to each other and calculate the amount of entanglement between the different optical and mechanical modes. We show that the composite system exhibits intercavity photon-phonon entanglement.

I. INTRODUCTION

Quantum cavity optomechanics capitalizes on the radiation pressure of light exerted on a mechanical degree of freedom in a cavity [1–3] to enable coupling between these different degrees of freedom. This currently highly active field of quantum physics is witnessing accelerated theoretical development [4–10] as well as significant experimental achievements [11–16]. More recently, an efficient quantum interface between optical photons and mechanical phonons has been illustrated [17]. Optomechanics serves as an excellent test bed for fundamental experiments at the quantum-classical boundary, leading to innovative ways of controlling the mutual interaction between light and the mechanical motion of mesoscopic objects. Sideband cooling to the ground state of mechanical resonator systems [18–20] is a challenge experimentally due to the unavoidable thermal coupling of the resonators to their environments. Nevertheless, these challenges have been overcome, with different experimental groups recently demonstrating cooling to the ground state of mechanical oscillators in cavity electromechanical and optomechanical systems [21–24]. Hence we are now in the era of quantum-mechanical control of macroscopic objects [25].

With the complete control of a single optomechanical system in sight, these systems can provide new tools for implementing quantum measurement schemes [26,27] and applications of a quantum photon-phonon interface [28,29]. Hence it is important to investigate the existence of entanglement between photons and phonons when we couple several of these systems together. Currently, the mechanical and optical modes within one optomechanical system have been shown to exhibit a considerable degree of entanglement [30–33]. The entanglement between the output optical fields of a trapped-mirror system has also been described [34]. A remarkable feature of optomechanical entanglement is that it can be present even at nonzero temperatures. Mazzola and Paternostro [35] showed the presence of entanglement between a pair of optomechanical cavities, in the linearized regime, that arises when each cavity is driven by one of the twin beams generated by a source of spontaneous parametric down conversion. The optomechanical systems become entangled due to quantum correlations in the light sources driving each cavity. Here we are going to take a different approach

and examine various entanglement properties between three different optomechanical cavities coupled via their optical ports in either a reversible or irreversible (cascaded) manner. An alternative approach would be to couple the mechanical resonators rather than the optical resonators [36]. A system of two coupled microwave cavities containing a mechanical element has also been considered recently by Heinrich and Marquardt [37]. The irreversible coupling has also recently been used to prepare entangled states in a driven cascaded quantum optical network [38]. We note that a similar scheme for generating distant optomechanical entanglement using reversible coupling between two cavities has recently been reported [39]. However, this approach, unlike ours, uses an adiabatic approximation resulting in quite different dynamics.

This paper is structured as follows. We begin with a description of the model in Sec. II describing the two couplings (reversible and irreversible) in which the optomechanical array can be set up. We then treat each coupling configuration in detail in Sec. III for different choices of the driving laser frequencies: First, in Secs. III A1 and III B1, we analyze the dynamics when each optomechanical cavity in the array is driven by a laser field of the same frequency. This detuning allows both squeezing and beam-splitter interactions between the optomechanical modes within each cavity. Our results show how the entanglement generated between intracavity modes can be distributed over intercavity modes in the presence of optical coupling between the different optomechanical cavities. Second, for each coupling configuration, we consider the case when the driving lasers of each cavity have different frequencies, in Secs. III A2 and III B2. We then choose particular detunings with respect to the mechanical frequency of each optomechanical unit to ensure that the source cavity is driven on the blue sideband and the receiver cavity is driven on the red sideband. This results in the field in the source cavity becoming entangled with the mechanical resonator in that cavity. The entanglement is then transferred to the mechanical resonator of the receiver cavity via the red sideband. We show that in this case, the composite system exhibits steady-state intercavity entanglement under the stability conditions for each optomechanical cavity. Finally, we summarize our results in Sec. IV.

II. THE MODEL

The basic idea in quantum cavity optomechanics is to induce a reversible coupling between an optical and mechanical resonator. Typically the interaction arises from the radiation

*uzma@physics.uq.edu.au

pressure of light. The usual setup is modeled as an optical cavity with its resonance frequency altered by the displacement of some mechanical resonator. A shift in the resonance frequency of the optical cavity changes the circulating power and thus changes the radiation pressure on the mechanical resonator, yielding the optomechanical coupling, which gives rise to a plethora of effects depending on how the various parameters and configurations are manipulated in the system. For example, the cavity can be driven to a steady-state amplitude and the nonlinear optomechanical interaction linearized around this amplitude. This gives a coupling that is quadratic in the amplitude of the optical and mechanical resonator. The goal in recent experiments has been to push the macroscopic mechanical elements of optomechanical systems towards the quantum limit by various passive and active cooling protocols.

A system of three coupled cavities could be considered as either a triangular or a linear topology for the optomechanical array. We choose to consider a composite system of a linear chain of two or three identical cavities where the optical and mechanical modes in each cavity are quadratically coupled to each other. Each cavity (1, 2, 3) is an optical Fabry-Perot cavity in which one of the mirrors is subject to a harmonic restoring force and can thus move due to radiation pressure. The trio of optomechanical cavities can be coupled together in two different configurations: via a *reversible* coupling or an *irreversible* coupling configuration, as illustrated in Fig. 1. The mechanical resonator in both cases has a frequency $\omega_{m_{1,2,3}}$ and damping rate $\mu_{1,2,3}$, while the optical cavity has a resonance frequency $\omega_{c_{1,2,3}}$ and is strongly driven with a coherent pump field at frequency $\omega_{L_{1,2,3}}$.

Reversible coupling allows a coherent photon exchange between nearest-neighbor optical ports, whereas the irreversible coupling is a forward feed method modeled using the cascaded systems approach [40,41]. Reversible coupling requires that the cavities be evanescently coupled and thus they must be close to each other; however, the irreversible (cascaded) coupling does not require this, but will require circulators to be placed between the optical cavities to ensure irreversibility.

The total Hamiltonian for the uncoupled optomechanical array in the Schrödinger picture is given by

$$H = \hbar \sum_{k=1}^{3} \omega_{c_k} a_k^\dagger a_k + \omega_{m_k} b_k^\dagger b_k + G_0 a_k^\dagger a_k (b_k + b_k^\dagger)$$
$$+ [E_k a_k^\dagger e^{-i\omega_{L_k} t} + E_k^* a_k e^{i\omega_{L_k} t}], \quad (1)$$

where a_k (b_k) and $a_k^\dagger$ ($b_k^\dagger$) are the annihilation and creation operators, respectively, of each optical (mechanical) mode, and E_k is the amplitude of the optical driving field of the kth cavity. We have assumed here that the cavities are identical such that the optomechanical coupling G_0 is the same. The master equation for the composite coupled system is given as

$$\frac{d\rho}{dt} = \frac{-i}{\hbar}[H,\rho] + \sum_{k=1}^{3} \kappa_k \mathcal{D}[a_k]\rho + \mu_k(\bar{n}+1)\mathcal{D}[b_k]\rho$$
$$+ \mu_k \bar{n} \mathcal{D}[b_k^\dagger]\rho + \mathcal{L}_{\mathrm{rev/irr}}, \quad (2)$$

where the optical bath modes are taken to be in the vacuum state and $\bar{n} = 1/(e^{\frac{\hbar \omega_m}{k_B T}} - 1)$ is the mechanical phonon bath occupation number. The linewidth of cavity k is given by κ_k and the mechanical damping rate is μ_k. The damping superoperator $\mathcal{D}[A]$ is defined by

$$\mathcal{D}[A]\rho = A\rho A^\dagger - \frac{1}{2}(A^\dagger A \rho + \rho A^\dagger A). \quad (3)$$
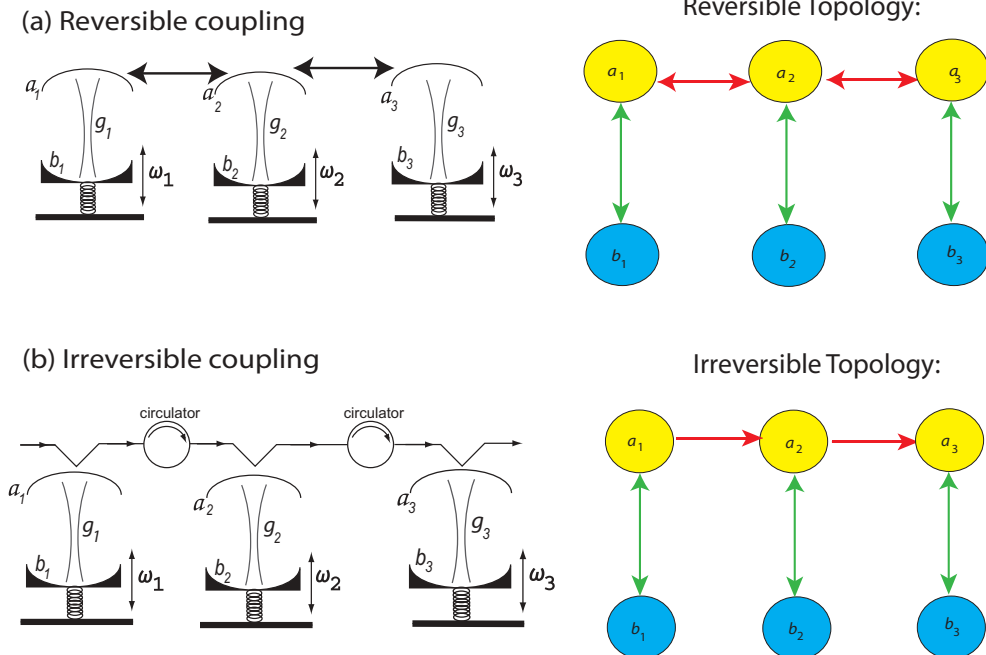

FIG. 1. (Color online) Model: The three optomechanical cavities can be coupled either (a) reversibly via coherent photon exchange (tunneling) between nearest neighbors or (b) irreversibly as forward feed using circulators. The array exhibits a different topology for each coupling configuration.

$\mathcal{L}_{\text{rev/irr}}$ is the coupling between the optomechanical cavities which can either be $\mathcal{L}_{\text{rev}}$, reversible, or $\mathcal{L}_{\text{irr}}$, irreversible. The reversible coupling is given as

$$\mathcal{L}_{\text{rev}} = -i\chi_{12}[a_1 a_2^\dagger + a_1^\dagger a_2, \rho] - i\chi_{23}[a_2 a_3^\dagger + a_3^\dagger a_2, \rho], \quad (4)$$

where χ_{jk} is an arbitrary coupling strength between the reversibly coupled nearest-neighbor cavities j and k. The irreversible coupling is a feed forward exchange only between the optical modes described by the cascaded systems approach [40–42] as

$$\mathcal{L}_{\text{irr}} = \sqrt{\kappa_1 \kappa_2}([a_1\rho, a_2^\dagger] + [a_2, \rho a_1^\dagger]) + \sqrt{\kappa_1\kappa_3}([a_1\rho, a_3^\dagger]$$
$$+ [a_3, \rho a_1^\dagger]) + \sqrt{\kappa_2\kappa_3}([a_2\rho, a_3^\dagger] + [a_3, \rho a_2^\dagger]). \quad (5)$$

We assume that the intercavity coupling is either reversible or irreversible, but not both together. As each cavity is externally driven, we linearize the radiation pressure interaction about the steady-state field amplitude in each cavity. We now consider in detail both coupling configurations under the effect of different optomechanical interactions induced between the mechanical and optical modes of each cavity in the optomechanical array.

III. COUPLED OPTOMECHANICAL ARRAYS

A. Reversible coupling

We first consider the reversible coupling configuration between a chain of up to three optomechanical cavities. Here the three cavities are evanescently coupled to nearest neighbors with an arbitrary coupling strength χ_{jk}, as given in Eq. (4). The topology we are considering here thus allows for a reversible exchange of optical excitations between the cavities, as shown in Fig. 1(a). We are interested in the presence and possible distribution of entanglement between interoptical and mechanical degrees of freedom across the array.

Starting from Eq. (1), we move to the interaction picture using the unitary transformation

$$U_0(t) = e^{-i\hbar(\omega_{L_1} a_1^\dagger a_1 + \omega_{L_2} a_2^\dagger a_2 + \omega_{L_3} a_3^\dagger a_3)t}, \quad (6)$$

which will give rise to a detuning, $\Delta_k = \omega_{c_k} - \omega_{L_k}$, between each cavity with respect to its corresponding driving laser frequency. Hence the steady-state cavity amplitudes, in the absence of the optomechanical interaction, are given by

$$\alpha_k = \frac{-iE_k}{\kappa_k/2 + i\Delta_k}. \quad (7)$$

Following the canonical transformation in the displaced reference frame, $\bar{a}_k = a_k - \alpha_k$, results in the effective Hamiltonian of the form

$$H_I = \hbar \sum_{k=1}^{3} \Delta_k \bar{a}_k^\dagger \bar{a}_k + \omega_{m_k} b_k^\dagger b_k + g_k(\bar{a}_k^\dagger + \bar{a}_k)(b_k + b_k^\dagger)$$
$$+ \hbar\chi_{12}(\alpha_1^* \bar{a}_2 e^{i(\omega_{L_1} - \omega_{L_2})t} + \alpha_1 \bar{a}_2^\dagger e^{-i(\omega_{L_1} - \omega_{L_2})t})$$
$$+ \hbar\chi_{23}(\alpha_2^* \bar{a}_3 e^{i(\omega_{L_2} - \omega_{L_3})t} + \alpha_2 \bar{a}_3^\dagger e^{-i(\omega_{L_2} - \omega_{L_3})t}), \quad (8)$$

where $g_k = \alpha_k G_0$ is the effective optomechanical coupling strength proportional to the steady-state amplitude of the cavity field due to linearization of the radiation pressure force. We note an additional driving term on each optical mode due to the steady-state coherent field leaking from its nearest neighbor.

This can be filtered out using a beam splitter and a coherent local oscillator, and we thus ignore it in our work. The resulting linearized master equation in the interaction picture for the system of three reversibly coupled optomechanical cavities is now

$$\frac{d\rho}{dt} = -\frac{i}{\hbar}[H_I, \rho] + \sum_{k=1}^{3} \kappa_k \mathcal{D}[\bar{a}_k]\rho + \mu_k(\bar{n}+1)\mathcal{D}[b_k]\rho$$
$$+ \mu_k \bar{n} \mathcal{D}[b_k^\dagger]\rho + \chi_{12}([\bar{a}_1\rho, \bar{a}_2^\dagger]e^{-i(\omega_{L_1} - \omega_{L_2})t}$$
$$+ [\bar{a}_2, \rho\bar{a}_1^\dagger]e^{i(\omega_{L_1} - \omega_{L_2})t}) + \chi_{23}([\bar{a}_2\rho, \bar{a}_3^\dagger]e^{-i(\omega_{L_2} - \omega_{L_3})t}$$
$$+ [\bar{a}_3, \rho\bar{a}_2^\dagger]e^{i(\omega_{L_2} - \omega_{L_3})t}), \quad (9)$$

where the reversible coupling terms introduced in Eq. (4) have been considered. The reversible coupling is analogous to a beam-splitter interaction between two modes. We have ignored any phase differences between the relative driving fields here. We will drop the bars from now on; however, we are working in the displaced picture, as evidenced by the appearance of the effective coupling strength g_k in the interaction Hamiltonian H_I. In the following, we consider different choices for the driving laser frequencies, such that each cavity may be blue or red detuned.

1. Equal driving laser frequencies with the full interaction Hamiltonian

We now consider the dynamics of the chain of reversibly coupled optomechanical systems such that the composite system evolves, as given by the full interaction Hamiltonian H_I in Eq. (8). We choose the frequencies on all driving laser fields to be the same, $\omega_{L_1} = \omega_{L_2} = \omega_{L_3} = \omega_L$. We can tune all driving fields to be simultaneously on the same sideband (i.e., all red or all blue). The master equation for this choice of equal laser frequencies is now

$$\frac{d\rho}{dt} = -\frac{i}{\hbar}[H_I, \rho] + \sum_{k=1}^{3} \kappa_k \mathcal{D}[\bar{a}_k]\rho + \mu_k(\bar{n}+1)\mathcal{D}[b_k]\rho$$
$$+ \mu_k \bar{n}\mathcal{D}[b_k^\dagger]\rho + \chi_{12}([\bar{a}_1\rho, \bar{a}_2^\dagger] + [\bar{a}_2, \rho\bar{a}_1^\dagger])$$
$$+ \chi_{23}([\bar{a}_2\rho, \bar{a}_3^\dagger] + [\bar{a}_3, \rho\bar{a}_2^\dagger]), \quad (10)$$

such that there are no time-dependent coefficients accompanying the reversible coupling terms. Note that this choice of laser frequencies requires that either $\omega_{L_k} = \omega_{c_k} - \omega_{m_k}$ (all cavities on the red sideband, $\Delta_k = \omega_{m_k}$) or $\omega_{L_k} = \omega_{c_k} + \omega_{m_k}$ (all cavities on the blue sideband, $\Delta_k = -\omega_{m_k}$).

As has been shown previously [33], intracavity photon-phonon entanglement is present within each optomechanical cavity. However, here we are interested in the presence of entanglement between the optical and mechanical resonators in distinct optomechanical cavities. Our composite system under study is in a Gaussian state as it starts from the vacuum, and the equations of motion are linear. Consequently, to quantify the entanglement, we can use the logarithmic negativity measure for Gaussian states formulated by Vidal [43]. The logarithmic negativity between two states is expressed in terms of the entries of their covariance matrix γ, which is a 4×4 matrix
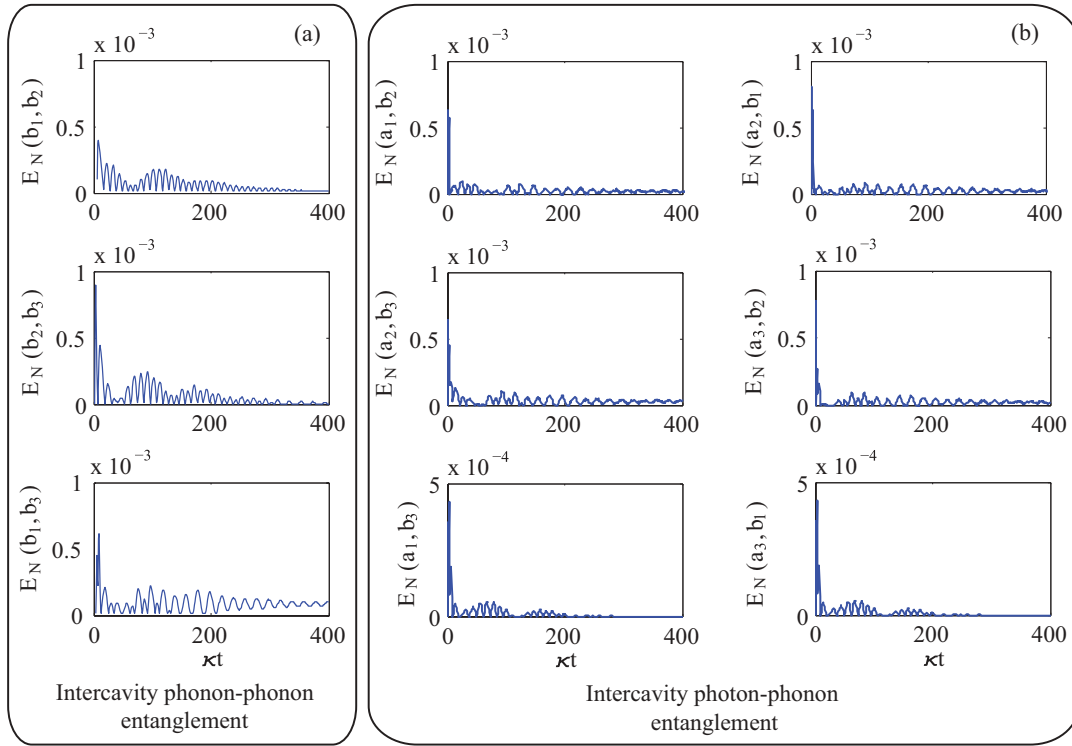
FIG. 2. (Color online) Reversible coupling with the full interaction. The temporal evolution of the entanglement, E_N, quantified by the logarithmic negativity between all possible selections of intercavity modes of the optomechanical array: (a) phonon-phonon and (b) photon-phonon, where we have chosen $\kappa_{1,2,3} = \kappa$, $\mu_{1,2,3}/\kappa = 0.01$, $\Delta_{1,2,3}/\kappa = \omega_{1,2,3}/\kappa = 200$, $g_{1,2,3}/\kappa = 0.5$, $\chi_{12}/\kappa = \chi_{23}/\kappa = 1$, and $\bar{n} = 0$.

given as

$$\gamma = \begin{pmatrix} \gamma_A & \gamma_C \\ \gamma_C^T & \gamma_B \end{pmatrix}, \quad \gamma_A, \gamma_B, \gamma_C \in M(2, \mathbb{R}). \quad (11)$$

The matrices $\gamma_{A,B}$ arise from position and momentum quadratures of the optical and mechanical modes, respectively, while γ_C is a result of cross terms between the optical and mechanical position and momentum quadratures. The logarithmic negativity is then calculated as

$$E_N = \begin{cases} -\ln f(\gamma)/2 & \text{if} \quad f(\gamma) < 1 \\ 0 & \text{otherwise,} \end{cases} \quad (12)$$

where the function $f : C(4) \longrightarrow \mathbb{R}^+$ is defined as

$$f(\gamma) = \Gamma_{A,B,C} - \sqrt{\Gamma_{A,B,C}^2 - |\gamma|}, \quad (13)$$

such that

$$\Gamma_{A,B,C} = \frac{|\gamma_A| + |\gamma_B|}{2} - |\gamma_C|, \quad (14)$$

where $|\gamma|$ is the determinant of γ.

Hence in order to determine the matrix elements of each 2×2 matrix, $\gamma_{A,B,C}$, we calculate the second-order moments from the master equation of the composite system. By inserting the relevant second-order moments into Eq. (12), we can determine the entanglement between any two modes of the system.

Figure 2(a) shows the entanglement quantified by the logarithmic negativity between the intercavity mechanical modes as a function of time where we have all parameters

in units of the cavity linewidth, κ. We see that the mirrors of different optomechanical cavities in the array are entangled in the absence of a direct coupling induced between them. Figure 2(b) shows the entanglement quantified by the logarithmic negativity between all two-mode intercavity photon-phonon combinations of the composite system of coupled optomechanical cavities. Clearly all six pairs of photon-phonon modes of the system are entangled with each other. We note the symmetry for pairs of oscillators a_j, b_k and a_k, b_j. This is due to the symmetry in the Hamiltonian, given by Eq. (8), for cavities with identical parameters ω_{m_k} and g_k.

When the three cavities are each detuned to the red sideband, we have found that the entanglement reaches a maximum (as a function of time) when the detuning is resonant with the mechanical frequency of each cavity, i.e., $\Delta_k = \omega_{m_k}$, as illustrated in Fig. 3(a) for Δ_1. We would like to remind the reader that even though this is red sideband detuning, the full linearized interaction Hamiltonian has been considered here [that is to say, we do not make the rotating wave approximation (RWA) at this point], so that the squeezing terms $\hat{a}_k \hat{b}_k$ and $\hat{a}_k^\dagger \hat{b}_k^\dagger$ also contribute towards the dynamics of the system and, in fact, are responsible for the presence of the entanglement within each optomechanical unit. Detuning the cavity to the blue sideband, $\Delta = -\omega_m$, one would expect to achieve strong entanglement. However, for the blue sideband driving, care should be taken to ensure that the steady state, about which we have linearized the radiation pressure interaction, remains stable. If we operate in a regime in which the RWA would be valid, the steady state on the blue sideband is unstable when $g < \sqrt{\kappa \mu}/2$ [44].
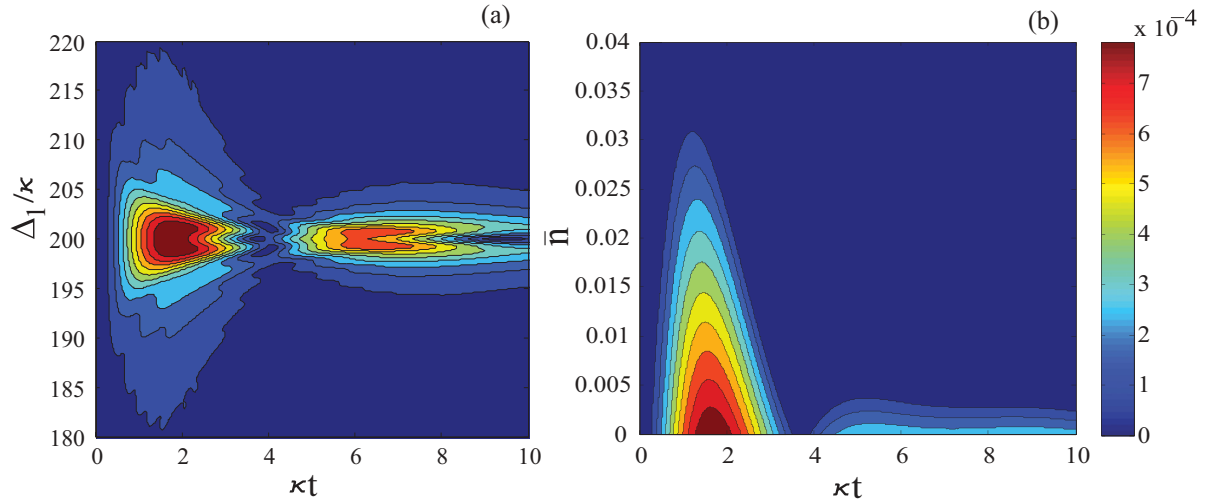
FIG. 3. (Color online) Reversible coupling with the full interaction. The temporal evolution of the entanglement, E_N, quantified by the logarithmic negativity between intercavity phonon modes b_1, b_2 of the optomechanical array as a function of (a) detuning of cavity 1, Δ_1, and (b) thermal occupation number $\bar{n}$, where we have chosen $\kappa_{1,2,3} = \kappa$, $\mu_{1,2,3}/\kappa = 0.01$, $\omega_1/\kappa = 200$, $\Delta_{2,3}/\kappa = \omega_{2,3}/\kappa = 200$, $g_{1,2,3}/\kappa = 0.5$, and $\chi_{12}/\kappa = \chi_{23}/\kappa = 1$.

Moreover, because we are operating in the resolved sideband regime, $\omega_m \gg \kappa, \mu$, the strength of the optomechanical coupling in each cavity, g_k, is restricted to very small values. As a result, for such weak-coupling parameters, the intracavity entanglement does not transfer to intercavity modes on the blue sideband.

If we tune to the red sideband, $\Delta = \omega_m$, so that the beam-splitter interaction is resonant, one would not expect much optical-mechanical entanglement within the RWA. However, for red sideband detuning, the stability conditions give $g < \frac{1}{2}\sqrt{\omega_m^2 + \frac{\mu^2 + \kappa^2}{4}}$. If the mechanical frequency ω_m is large enough, this enables one to use large values of g and remain within a stable operating regime. Under those conditions, it would not be valid to make the RWA, and thus the nonresonant terms cannot be neglected, resulting in entanglement between the optical and mechanical modes, even though we are driving on the red sideband. This results in an exchange of excitations on the optomechanical branches of the chain of oscillators, consequently distributing the intracavity entanglement between oscillators of different cavities due to the coupling between the optical ports. Hence the coupling between the optomechanical units facilitates the distribution of intracavity entanglement over the intercavity optical and mechanical modes.

Figure 3(b) shows how the intercavity phonon entanglement varies with an increase in thermal phonon number, $\bar{n}$, of the mechanics. Clearly each mechanical mode of the coupled optomechanical array will need to be as close as possible to its ground state to maintain the intercavity phonon-phonon entanglement induced by the reversible coupling between the optical modes.

2. Unequal driving laser frequencies

So far we have looked at the distribution of entanglement in optomechanical arrays in the reversible coupling under the full interaction Hamiltonian, such that optomechanical entanglement was generated within each cavity independently. We are now interested in the distribution of entanglement in optomechanical arrays given that we have entanglement generated only in the source cavity by tuning to the blue sideband. For simplicity, we consider a chain of only two coupled cavities here; however, our results can be extended for a large number of similarly coupled optomechanical systems. We choose the source cavity to be exclusively on the blue sideband and the receiver cavity to be only on the red sideband.

We consider the cavities to be on resonance so that $\omega_{c_1} = \omega_{c_2} = \omega_c$, and assume the mechanical resonators have the same frequency, $\omega_{m_1} = \omega_{m_2} = \omega_m$, but as we drive cavity 1 on the blue sideband, $\Delta_1 = \omega_c - \omega_{L_1} = -\omega_m$, and cavity 2 on the red sideband, $\Delta_2 = \omega_c - \omega_{L_2} = \omega_m$. This choice then implies $\omega_c = \frac{\omega_{L_1} + \omega_{L_2}}{2}$ for the optical frequencies and $\omega_m = \frac{(\omega_{L_1} - \omega_{L_2})}{2}$ for mechanical frequencies. However, there will be a detuning created by the different driving laser frequencies, $\omega_{L_1} \neq \omega_{L_2}$. We now go to another interaction picture with respect to the mechanical frequency ω_m and make the RWA so that the interaction Hamiltonian of the composite system for this coupling configuration is

$$\acute{H}_I = \hbar g_1(a_1 b_1 + a_1^\dagger b_1^\dagger) + \hbar g_2(a_2^\dagger b_2 + a_2 b_2^\dagger), \quad (15)$$

and the master equation in the RWA now will be given as

$$\frac{d\rho}{dt} = -\frac{i}{\hbar}[\acute{H}_I, \rho] + \sum_{k=1}^{2} \kappa_k \mathcal{D}[a_k]\rho + \mu_k(\bar{n}+1)\mathcal{D}[b_k]\rho$$
$$+ \mu_k \bar{n} \mathcal{D}[b_k^\dagger]\rho - i\chi_{12}[a_1 a_2^\dagger + a_2 a_1^\dagger, \rho]. \quad (16)$$

Here, in the source cavity, the optomechanical interaction is a two-mode squeezing interaction, which will entangle the mechanics and the field. Tuning the receiver optomechanical cavity to the red sideband, we generate a beam-splitter interaction, which can swap the state of the mechanics and the field. Thus we can use the first cavity to entangle the mirror motion
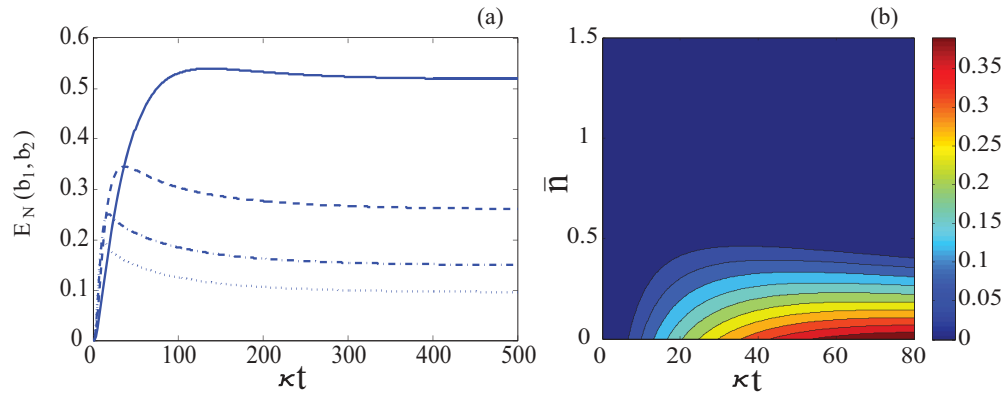
FIG. 4. (Color online) Reversible coupling with cavity 1 blue detuned and cavity 2 red detuned. The temporal evolution of entanglement, E_N, quantified by the logarithmic negativity between the intercavity phonons of two optomechanical cavities (b_1,b_2), where we have chosen $\kappa_{1,2} = \kappa$, $\mu_{1,2}/\kappa = 0.01$, $g_1/\kappa = 0.02$, and $\chi_{12}/\kappa = 1$, (a) with $\bar{n} = 0$ and different g_2/κ: 0.1 (solid line), 0.2 (dashed line), 0.3 (dashed dotted line), and 0.4 (dotted line), and (b) as a function of thermal phonon number $\bar{n}$ with $g_2/\kappa = 0.1$.

and the field, take the field out via the reversible coupling, and then swap it into the mirror motion in the second cavity. Hence this system is capable of generating entanglement between the mechanical resonators, b_1 and b_2, even though the receiver cavity is explicitly on the red sideband.

We illustrate this in Fig. 4(a), which shows how the entanglement varies between the two resonators, b_1 and b_2, as a function of time with dimensionless parameters for different optomechanical coupling strengths g_2 for a fixed g_1. We note for this coupling configuration that the entanglement between intercavity phonons becomes larger for weaker optomechanical coupling of cavity 2, which is on the red sideband. Figure 4(b) shows how the temporal intercavity phonon entanglement varies with the phonon occupation number $\bar{n}$. While there is still significant entanglement in this coupling for nonzero $\bar{n}$, here again we find that the mechanical resonators of the coupled optomechanical system would need to remain close to their respective ground states to stay entangled with each other.

Clearly, from Fig. 4(a), the entanglement in the composite system here is much larger in magnitude from the previous case of the full linearized interaction Hamiltonian. For this coupling configuration, we find that the system goes to a steady state and hence we evaluate the steady-state second-order moments and calculate the logarithmic negativity between the mechanical modes for both cavities. We plot the steady-state entanglement quantified by the logarithmic negativity between the resonators b_1,b_2 versus the two optomechanical coupling strengths, g_1 and g_2 in Fig. 5(a). We choose parameters for both cavities such that the respective stability conditions are satisfied in the steady state.

Finally, for the reversible coupling configuration, Fig. 5(b) shows that the steady-state entanglement between intercavity phonon modes increases with the strength of the reversible coupling χ_{12} between the optical modes. We note from Fig. 5(b) that the entanglement does not linearly increase with g_2. The correlation $\langle b_2 b_1 \rangle$ and thus the intercavity entanglement arise from the state swap (arising from the form
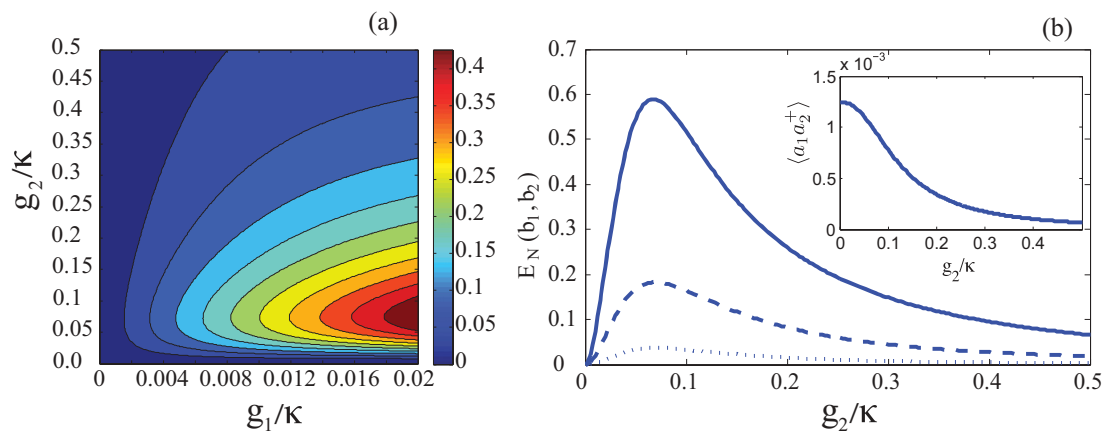

FIG. 5. (Color online) Reversible coupling with cavity 1 blue detuned and cavity 2 red detuned. The steady-state entanglement E_N quantified by the logarithmic negativity between the intercavity phonons of two optomechanical cavities (b_1,b_2), where we have chosen $\kappa_{1,2} = \kappa$, $\mu_{1,2}/\kappa = 0.01$ and $\bar{n} = 0$, (a) as a function of g_1/κ and g_2/κ for $\chi_{12}/\kappa = 1$, and (b) as a function of g_2/κ for $g_1 = 0.02$ and different χ_{12}/κ: 1 (solid line), 0.5 (dashed line), and 0.2 (dotted line). The inset shows the correlation $\langle a_1 a_2^\dagger \rangle$ as a function of g_2/κ for the same parameters, except for $\chi_{12}/\kappa = 1$ and $g_1/\kappa = 0.02$.

of the red sideband coupling) between a_2 and b_2, once the field has been transferred from the optical mode a_1 to a_2. Initially, as g_2 increases, the entanglement $E_N(b_1,b_2)$ also increases. However, for larger g_2, the rate of the state swap between a_2 and b_2 becomes close to and eventually faster than the coupling between a_1 and a_2, which is restricted by the fixed coupling parameter χ_{12}. Consequently, this results in a decay of the correlation $\langle a_1 a_2^\dagger \rangle$ and hence $E_N(b_1,b_2)$ along the g_2 axis. As the results show, there is therefore an optimum combination of g_1 and g_2 for which the intercavity phonons are maximally entangled in the steady state before logarithmic negativity begins to decrease with increasing g_2.

B. Forward feed (irreversible) coupling

We now investigate the presence and possible distribution of entanglement between intercavity modes in the forward feed coupling configuration. Here the cavities are coupled via a unidirectional coupling only. In our calculations, we have neglected the time delay between the cavities. Effectively, we can consider cavity 1 as the "main source" cavity, while cavity 3 is only a receiver cavity. Cavity 2, on the other hand, receives photons from cavity 1 as well as drives cavity 3. The topology of our setup in this coupling configuration is further illustrated in Fig. 1(b). Hence we have reversible interactions between the optomechanical branches of the chain, but irreversible interactions between the optical ports coupling the individual optomechanical units. This is quite a different configuration compared to previous work on coupled oscillator arrays [45]. We have for the interaction Hamiltonian

$$
\begin{aligned}
H_I = {}& \hbar \sum_{k=1}^{3} \Delta_k \bar{a}_k^\dagger \bar{a}_k + \omega_{m_k} b_k^\dagger b_k + g_k(\bar{a}_k^\dagger + \bar{a}_k)(b_k + b_k^\dagger) \\
& + \hbar\sqrt{\kappa_1 \kappa_2}(\alpha_1^* \bar{a}_2 e^{i(\omega_{L_1}-\omega_{L_2})t} + \alpha_1 \bar{a}_2^\dagger e^{-i(\omega_{L_1}-\omega_{L_2})t}) \\
& + \hbar\sqrt{\kappa_2 \kappa_3}(\alpha_2^* \bar{a}_3 e^{i(\omega_{L_2}-\omega_{L_3})t} + \alpha_2 \bar{a}_3^\dagger e^{-i(\omega_{L_2}-\omega_{L_3})t}) \\
& + \hbar\sqrt{\kappa_1 \kappa_3}(\alpha_1^* \bar{a}_3 e^{i(\omega_{L_1}-\omega_{L_3})t} + \alpha_1 \bar{a}_3^\dagger e^{-i(\omega_{L_1}-\omega_{L_3})t}),
\end{aligned}
\tag{17}
$$

where $\Delta_k = \omega_{c_k} - \omega_{L_k}$ is the detuning of each cavity with respect to the driving laser field. As before, we have an additional driving [last three terms in Eq. (17)] on each receiver cavity (2,3) due to the steady-state coherent field leaking from each source cavity (1,2), which can be filtered out, and we thus ignore it in our work. In Eq. (17), g_k is now the effective optomechanical coupling strength proportional to the steady-state amplitude of the cavity field due to linearization of the radiation pressure force. Following the canonical transformation in the displaced reference frame, $\bar{a}_k = a_k - \alpha_k$, the master equation in the interaction picture for the cascaded system of three optomechanical cavities is now

$$
\begin{aligned}
\frac{d\rho}{dt} = {}& -\frac{i}{\hbar}[H_I,\rho] + \sum_{k=1}^{3} \kappa_k \mathcal{D}[\bar{a}_k]\rho + \mu_k(\bar{n}+1)\mathcal{D}[b_k]\rho \\
& + \mu_k \bar{n} \mathcal{D}[b_k^\dagger]\rho + \sqrt{\kappa_1 \kappa_2}([\bar{a}_1\rho,\bar{a}_2^\dagger]e^{-i(\omega_{L_1}-\omega_{L_2})t} \\
& + [\bar{a}_2,\rho\bar{a}_1^\dagger]e^{i(\omega_{L_1}-\omega_{L_2})t}) + \sqrt{\kappa_2 \kappa_3}([\bar{a}_2\rho,\bar{a}_3^\dagger]e^{-i(\omega_{L_2}-\omega_{L_3})t} \\
& + [\bar{a}_3,\rho\bar{a}_2^\dagger]e^{i(\omega_{L_2}-\omega_{L_3})t}) + \sqrt{\kappa_1 \kappa_3}([\bar{a}_1\rho,\bar{a}_3^\dagger]e^{-i(\omega_{L_1}-\omega_{L_3})t} \\
& + [\bar{a}_3,\rho\bar{a}_1^\dagger]e^{i(\omega_{L_1}-\omega_{L_3})t}).
\end{aligned}
\tag{18}
$$

We have ignored any phase differences between the relative driving fields here. From now on, we drop the bars from the operators but we will be working in the displaced picture and hence consider the effective optomechanical coupling strength g_k. In the following, we consider different choices for the driving laser frequencies, such that each cavity may be blue or red detuned.

1. Equal driving laser frequencies with the full interaction in Hamiltonian

First, we will consider the three optomechanical systems coupled in a cascaded fashion such that the composite system evolves, as given by the full interaction Hamiltonian H_I in Eq. (17). We choose the frequencies on all driving laser fields to be the same, $\omega_{L_1} = \omega_{L_2} = \omega_{L_3} = \omega_L$. We can tune all driving fields to be simultaneously on the same sideband (i.e., all red or all blue). The master equation for this choice of equal laser frequencies is

$$
\begin{aligned}
\frac{d\rho}{dt} = {}& -\frac{i}{\hbar}[H_I,\rho] + \sum_{k=1}^{3} \kappa_k \mathcal{D}[a_k]\rho + \mu_k(\bar{n}+1)\mathcal{D}[b_k]\rho \\
& + \mu_k \bar{n} \mathcal{D}[b_k^\dagger]\rho + \sqrt{\kappa_1 \kappa_2}([a_1\rho,a_2^\dagger] + [a_2,\rho a_1^\dagger]) \\
& + \sqrt{\kappa_2 \kappa_3}([a_2\rho,a_3^\dagger] + [a_3,\rho a_2^\dagger]) \\
& + \sqrt{\kappa_1 \kappa_3}([a_1\rho,a_3^\dagger] + [a_3,\rho a_1^\dagger]),
\end{aligned}
\tag{19}
$$

such that there are no time-dependent coefficients accompanying the forward feed coupling terms. As in the reversible coupling case, this choice of laser frequencies places the restriction that either $\omega_L = \omega_{c_k} - \omega_{m_k}$ (all red, $\Delta_k = \omega_{m_k}$) or $\omega_L = \omega_{c_k} + \omega_{m_k}$ (all cavities on the blue sideband, $\Delta_k = -\omega_{m_k}$).

Figure 6(a) shows the existence of pairwise entanglement between the intercavity mechanical modes, b_1, b_2, and b_3, of the composite system for the forward feed coupling between the optical ports. Figure 6(b) shows the existence of entanglement between all possible pairs of the optical and mechanical modes of different cavities, i.e., intercavity photon-phonon entanglement in the composite system. Again, all six pairs of photon-phonon modes of the system are entangled with each other.

When the three cavities are each detuned to the red sideband, we have found the intercavity entanglement is maximum when the detuning is resonant with the mechanical frequency of each cavity, i.e., $\Delta_k = \omega_{m_k}$, as illustrated in Fig. 7(a) for Δ_1. As previously shown, the full linearized interaction Hamiltonian has been considered here, such that again the system is limited by different stability conditions on the blue and red sidebands, as discussed in Sec. III A 1. Hence the intercavity entanglement is found to exist only on the red sideband of the system, as the beam-splitter part of the Hamiltonian induces the distribution of the intracavity optomechanical entanglement between the cavity modes, under large values of the optomechanical coupling strength, g_k, allowed by the stability conditions of the system. Thus the forward feed coupling between the optomechanical units also facilitates the distribution of intracavity entanglement over the intercavity modes.

Figure 7(b) shows how the entanglement varies with an increase in mechanical thermal phonon number, $\bar{n}$. Clearly each mechanical mode of the coupled optomechanical array will
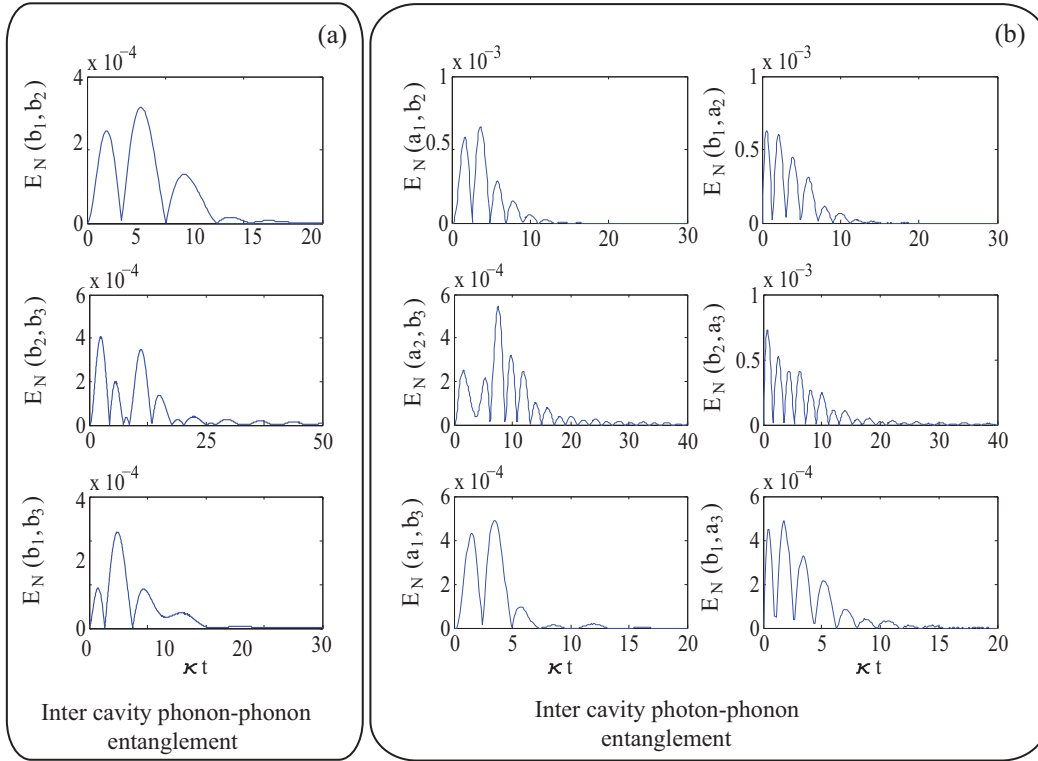
FIG. 6. (Color online) Forward feed coupling with the full interaction. The temporal evolution of the entanglement, E_N, quantified by the logarithmic negativity between all possible intercavity modes of the optomechanical array: (a) phonon-phonon and (b) photon-phonon, where we have chosen $\kappa_{1,2,3} = \kappa$, $\mu_{1,2,3}/\kappa = 0.01$, $\Delta_{1,2,3}/\kappa = \omega_{1,2,3}/\kappa = 400$, $g_{1,2,3}/\kappa = 0.5$, and $\bar{n} = 0$.

need to be as close as possible to its ground state to maintain the intercavity phonon-phonon entanglement induced by the forward feed coupling between the optical modes.

2. Unequal driving laser frequencies

Analogous to the reversible case, we are now interested in the distribution of entanglement in optomechanical arrays

given that we have entanglement generated only in the source cavity. Again, for simplicity, we consider a chain of only two coupled cavities here; however, our results can be extended for a large number of similarly coupled optomechanical systems. We choose the source cavity to be exclusively on the blue sideband and the receiver cavity also to be only on the red sideband and have the same conditions for the cavity frequencies and the detunings as in Sec. III A 2, such that the
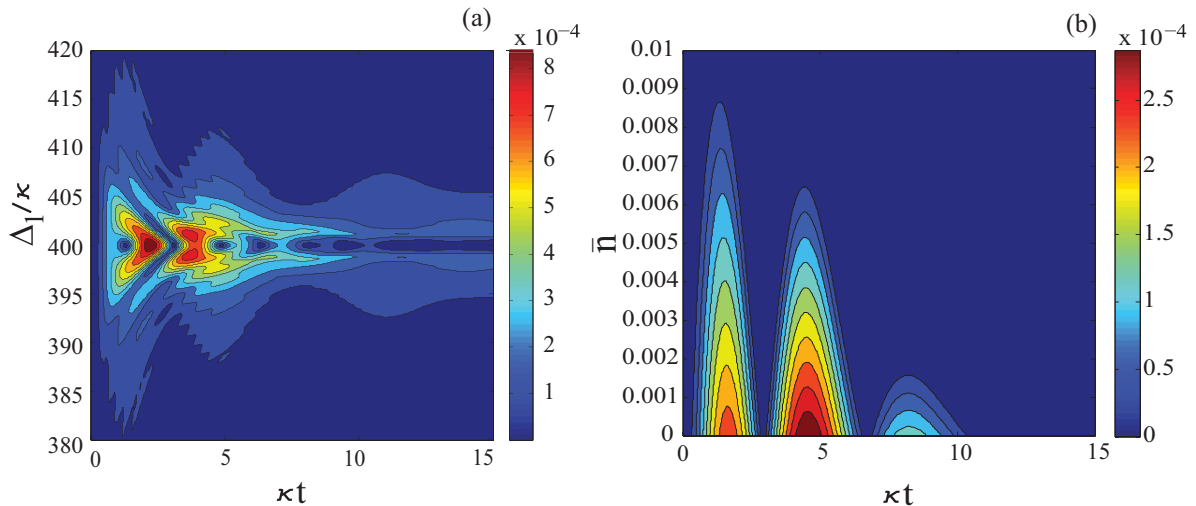

FIG. 7. (Color online) Forward feed coupling with the full interaction. The temporal entanglement E_N quantified by the logarithmic negativity between intercavity phonons b_1,b_2 of the optomechanical array as a function of (a) detuning of cavity 1, Δ_1, and (b) thermal occupation number $\bar{n}$, where we have chosen $\kappa_{1,2,3} = \kappa$, $\mu_{1,2,3}/\kappa = 0.01$, $\omega_1/\kappa = 400$, $\Delta_{2,3}/\kappa = \omega_{2,3}/\kappa = 400$, $g_{1,2,3}/\kappa = 0.5$, and $\bar{n} = 0$.
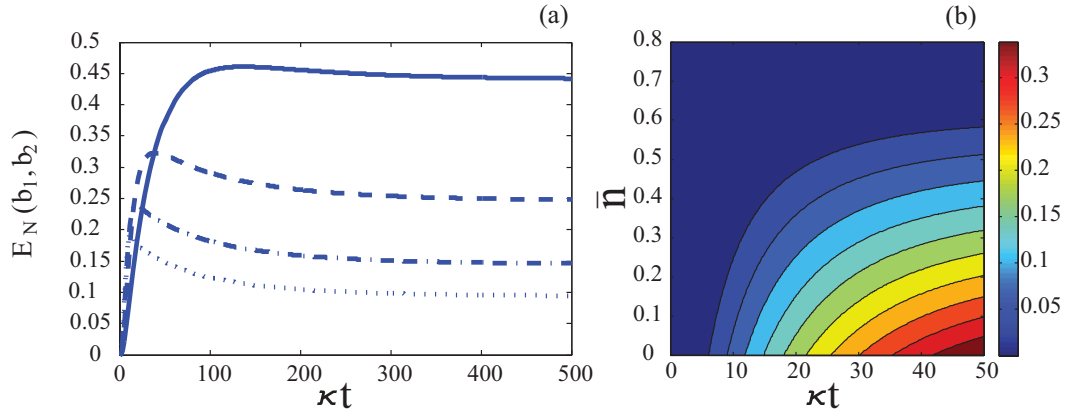
FIG. 8. (Color online) Forward feed coupling with cavity 1 blue detuned and cavity 2 red detuned. The temporal evolution of entanglement, E_N, quantified by the logarithmic negativity between the intercavity phonons of two optomechanical cavities (b_1,b_2), where we have chosen $\kappa_{1,2} = \kappa$, $\mu_{1,2}/\kappa = 0.01$, $g_1/\kappa = 0.02$, (a) with $\bar{n} = 0$ and different g_2/κ: 0.1 (solid line), 0.2 (dashed line), 0.3 (dashed dotted line), and 0.4 (dotted line), and (b) as a function of thermal phonon number $\bar{n}$ with $g_2/\kappa = 0.1$.

master equation in the RWA for the forward feed coupling now will be given as

$$\frac{d\rho}{dt} = -\frac{i}{\hbar}[\acute{H}_I, \rho] + \sum_{k=1}^{2} \kappa_i \mathcal{D}[a_k]\rho + \mu_k(\bar{n} + 1)\mathcal{D}[b_k]\rho$$
$$+ \mu_k \bar{n} \mathcal{D}[b_k^{\dagger}]\rho + \sqrt{\kappa_1 \kappa_2}([a_1\rho, a_2^{\dagger}] + [a_2, \rho a_1^{\dagger}]), \quad (20)$$

where, making the rotating wave approximation at the frequencies, $\Delta_1 = -\omega_m$ and $\Delta_2 = \omega_m$, the time-dependent coefficients in the coupling terms will be removed again. As before, the squeezing interaction between the optical and mechanical modes in the source cavity generates entanglement, which can be distributed along the chain in the array by taking the field out in the forward feed coupling and then swapping it into the mirror motion in the second cavity. Hence this system is capable of generating entanglement between the mechanical resonators, b_1 and b_2, even though the receiver cavity is explicitly on the red sideband.

We illustrate this in Fig. 8(a), which shows how the entanglement varies between the two resonators as a function of time with all parameters in units of κ for different optomechanical coupling strengths g_2 and for a fixed value of g_1. As before, the entanglement between b_1 and b_2 becomes larger in the weak-coupling regime of the receiver optomechanical system. In Fig. 8(b), we show how the intercavity phonon-phonon entanglement varies in this coupling configuration under the effect of increasing the mechanical thermal phonon number.

Here also we note that the intercavity entanglement quantified by the logarithmic negativity between the different modes is much larger compared to the case with the full linearized interaction Hamiltonian. We find the composite system has a steady state in this coupling configuration. Figure 9(a) shows the steady-state entanglement between b_1 and b_2 as a function of different values of the optomechanical coupling strength of each cavity g_k. Figure 9(b) shows how the correlation between the optical modes a_1 and a_2 scales with g_2 for a fixed value of g_1. Similar to the reversible configuration, increasing g_2 leads to a much faster state swap between a_2 and b_2 such that
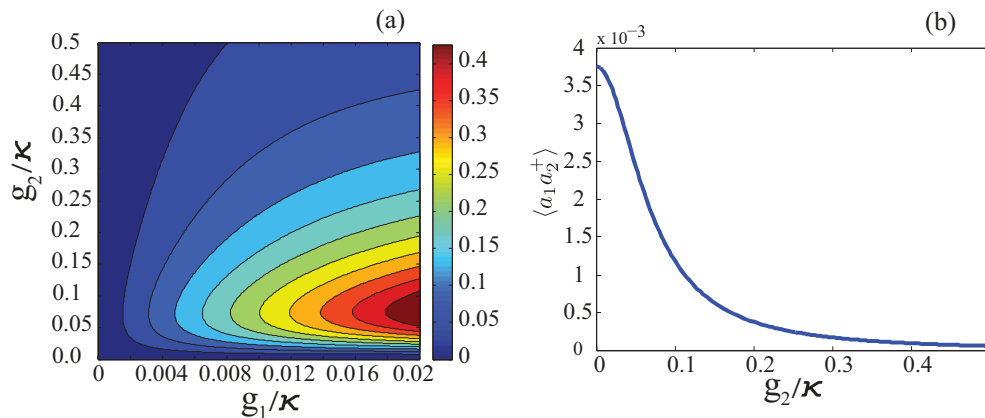

FIG. 9. (Color online) Forward feed coupling with cavity 1 blue detuned and cavity 2 red detuned. (a) The steady-state entanglement E_N quantified by the logarithmic negativity between the intercavity phonons of two optomechanical units (b_1,b_2) vs g_1/κ and g_2/κ, where we have chosen $\kappa_{1,2} = \kappa$, $\mu_{1,2}/\kappa = 0.01$, and $\bar{n} = 0$. (b) The steady-state correlation $\langle a_1 a_2^{\dagger}\rangle$ as a function of g_2/κ with the same parameters but with $g_1/\kappa = 0.02$.

the intercavity correlation between the optical modes, $\langle a_1 a_2^\dagger \rangle$, goes to zero along the g_2 axis.

We note that the steady-state results for the reversible and irreversible coupling configurations given in Figs. 5(b) and 9(a) appear to be identical. The effective coupling between the cascaded cavities in the reversible case is proportional to χ_{12}, while in the irreversible case, it is proportional to $\sqrt{\kappa_1 \kappa_2}$. However, the similarity is for the special case when the $\chi_{12} = \sqrt{\kappa_1 \kappa_2} = 1$, as chosen in Figs. 5(b) and 9(a). The equations of motion resulting from each configuration are, in fact, different in the coupling terms and give different results for different values of the coupling parameters, χ_{12} and $\sqrt{\kappa_1 \kappa_2}$. One can see this from the quantum stochastic differential equations for each coupling configuration given in the Appendix.

IV. SUMMARY

We have analyzed intercavity entanglement in an optomechanical array comprised of three coupled cavities, taking into account both a reversible coupling case via nearest-neighbor evanescent coupling between the optical modes as well as a forward feed model realized through the cascaded systems approach. Further, for each coupling, we have considered the effect of working with the full linearized interaction Hamiltonian (that is to say, without making the rotating wave approximation), such that both squeezing and beam-splitter optomechanical interactions are present. The dynamics of such a coupled optomechanical array show that intracavity optomechanical entanglement generated independently in each cavity can be distributed pairwise between intercavity photons as well as phonons. The topology of the chain of oscillators considered in this paper comprised of reversible optomechanical coupling between light and mechanics, alongside irreversible forward feed coupling between optical ports, is quite distinct from earlier results on coupled oscillators.

Moreover, for both irreversible and reversible configurations, we also considered external coherent laser driving of each cavity such that the source cavity is explicitly driven on the blue sideband, while the receiver cavity is only red detuned. In this choice of cavity-laser detunings, entanglement is only generated in the source cavity, while the receiver optical port simply swaps the entanglement from the field to the mechanics so that the mirrors b_1 and b_2 in the array become entangled. We find in this configuration that the intercavity entanglement generated is much larger and exists in the steady state. It then varies with the optomechanical coupling strengths g_1 and g_2 within each optomechanical cavity. For the reversible coupling configuration, the steady-state cross cavity phonon-phonon entanglement increases with the reversible optical coupling strength χ_{12} while in a region of stability of each system as defined by the respective rotating wave approximations on the blue and red sideband of the optomechanical cavities.

We also considered thermal effects on the entanglement generated in each case. It turns out that the mechanical modes will need to be in the ground state to achieve intercavity phonon-phonon entanglement, but can also exhibit some degree of entanglement with a small nonzero value of the phonon occupation number. While we illustrated the idea for only two cavities, this scheme can be extended to a chain of similarly coupled optomechanical units where the entanglement is generated only in the source unit but distributed along the entire chain due to state swap between the optics and mechanics. Here we have neglected delay effects in the forward feed case, which means that delays must be less than the cavity decay times, which sets the time scale for the dynamics of the optomechanical array. Even with this assumption, the forward feed case enables the optical cavities to be much further apart—up to one meter—than the reversible coupling case. Coupled optomechanical arrays could have wide applications as components of quantum repeaters and quantum memories required in quantum information processing.

APPENDIX

1. Reversible coupling

We have looked at the dynamics of the optomechanical arrays numerically, solving the master equation. In order to explain the steady-state behavior of the system, we evaluate the steady-state correlations between the intercavity phonons in this appendix via the quantum stochastic differential equations for the coupled cavities. To keep the analytical calculations feasible, we will only consider two cavities here, coupled reversibly with the source driven on only the blue sideband and the receiver cavity on the red sideband, i.e., driving the system with different laser frequencies on each optomechanical unit. Going into the interaction picture with respect to the driving laser fields, the collective system of the four oscillators can be described by the following closed set of coupled Langevin equations:

$$\frac{da_1}{dt} = -ig_1 b_1^\dagger - \frac{\kappa_1}{2} a_1 - i\chi_{12} a_2 + \sqrt{\kappa_1} a_{in}, \quad \text{(A1)}$$

$$\frac{da_2}{dt} = -ig_2 b_2 - \frac{\kappa_2}{2} a_2 - i\chi_{12} a_1 + \sqrt{\kappa_2} a_{in}, \quad \text{(A2)}$$

$$\frac{db_1^\dagger}{dt} = ig_1 a_1 - \frac{\mu_1}{2} b_1^\dagger + \sqrt{\mu_1} b_{1,in}^\dagger, \quad \text{(A3)}$$

$$\frac{db_2}{dt} = -ig_2 a_2 - \frac{\mu_2}{2} b_2 + \sqrt{\mu_2} b_{2,in}, \quad \text{(A4)}$$

where a_{in} is the vacuum input noise to the source cavity a_1, and $b_{k,in}$ is the noise for each mechanical resonator b_k. These linear equations can be solved analytically setting the time derivatives to zero, and employed to calculate all steady-state correlations that exist between the different oscillators in the collective system. Eliminating both cavity fields, we arrive at the following coupled quantum stochastic differential equations for the mechanical resonators b_1, b_2 only:

$$\frac{db_1}{dt} = -\frac{\gamma_1}{2} b_1 + i\chi'_{12} b_2^\dagger + \eta_1^* a_{in}^\dagger + \sqrt{\mu_1} b_{1,in}, \quad \text{(A5)}$$

$$\frac{db_2}{dt} = -\frac{\gamma_2}{2} b_2 + i\chi'_{12} b_1^\dagger - \eta_2 a_{in} + \sqrt{\mu_2} b_{2,in}, \quad \text{(A6)}$$

where $\gamma_1 = \mu_1 - \Gamma_1$ and $\gamma_2 = \mu_2 + \Gamma_2$, such that

$$\Gamma_k = \frac{4g_k^2 \kappa_j}{\kappa_k \kappa_j + 4\chi_{jk}^2}, \tag{A7}$$

$$\acute{\chi}_{kj} = \frac{4\chi_{kj} g_k g_j}{\kappa_k \kappa_j + 4\chi_{kj}^2}, \tag{A8}$$

$$\eta_k = \frac{4\chi_{kj} g_k \sqrt{\kappa_j} + 2i g_k \kappa_j \sqrt{\kappa_k}}{\kappa_k \kappa_j + 4\chi_{kj}^2}, \tag{A9}$$

where k, j refer to the two reversibly coupled cavities under consideration. To solve for the steady-state correlation functions, we evaluate the expression

$$\frac{d(b_2 b_1)}{dt} = \left(\frac{db_2}{dt}\right) b_1 + b_2 \left(\frac{db_1}{dt}\right) = 0, \tag{A10}$$

which gives

$$\langle b_2 b_1 \rangle = \frac{2i \acute{\chi}_{12}(1 + \langle b_1^\dagger b_1 \rangle + \langle b_2^\dagger b_2 \rangle)}{\gamma_1 + \gamma_2}. \tag{A11}$$

Equation (A11) shows the presence of a nonzero steady-state correlation and hence entanglement between the mechanical resonators b_1 and b_2. We note that increasing the reversible coupling strength χ_{12} will enhance the correlation and thus the entanglement, as seen in Fig. 5(b).

2. Irreversible coupling

Analogous to the reversible coupling, to examine the steady-state behavior of the irreversible coupling, we analyze the quantum stochastic differential equations for two coupled cavities where the first is blue detuned while the second is red detuned. Going into the interaction picture with respect to the driving laser fields, the collective system of the four

oscillators can be described by the following closed set of coupled Langevin equations:

$$\frac{da_1}{dt} = -ig_1 b_1^\dagger - \frac{\kappa_1}{2} a_1 + \sqrt{\kappa_1} a_{in}(t - \tau), \tag{A12}$$

$$\frac{da_2}{dt} = -ig_2 b_2 - \frac{\kappa_2}{2} a_2 - \sqrt{\kappa_1 \kappa_2} a_1(t - \tau) + \sqrt{\kappa_2} a_{\rm in}, \tag{A13}$$

$$\frac{db_1^\dagger}{dt} = ig_1 a_1 - \frac{\mu_1}{2} b_1^\dagger + \sqrt{\mu_1} b_{1,\rm in}^\dagger, \tag{A14}$$

$$\frac{db_2}{dt} = -ig_2 a_2 - \frac{\mu_2}{2} b_2 + \sqrt{\mu_2} b_{2,\rm in}, \tag{A15}$$

where τ is the time delay between the irreversibly coupled cavities. However, here we neglect any time delays, and set $\tau = 0$. As before, by eliminating both cavity fields, we arrive at the following coupled quantum stochastic differential equations for the mechanical resonators b_1 and b_2 only:

$$\frac{db_1^\dagger}{dt} = -\frac{\tilde{\gamma}_1}{2} b_1 + i\sqrt{\tilde{\Gamma}_1} a_{\rm in}^\dagger + \sqrt{\mu_1} b_{1,\rm in}^\dagger, \tag{A16}$$

$$\frac{db_2}{dt} = -\frac{\tilde{\gamma}_2}{2} b_2 + \sqrt{\tilde{\Gamma}_1 \tilde{\Gamma}_2} b_1^\dagger + i\sqrt{\tilde{\Gamma}_2} a_{\rm in} + \sqrt{\mu_2} b_{2,\rm in}, \tag{A17}$$

where $\tilde{\gamma}_1 = \mu_1 - \tilde{\Gamma}_1$, $\tilde{\gamma}_2 = \mu_2 + \tilde{\Gamma}_2$, and $\tilde{\Gamma}_k = \frac{4g_k^2}{\kappa_i}$, with $k = 1, 2$. Again using Eq. (A10), we arrive at the steady-state correlation between b_1 and b_2,

$$\langle b_2 b_1 \rangle = \frac{2\sqrt{\tilde{\Gamma}_1 \tilde{\Gamma}_2}}{\tilde{\gamma}_1 + \tilde{\gamma}_2} \langle b_1^\dagger b_1 \rangle, \tag{A18}$$

which accounts for the intercavity steady-state entanglement between the mechanical modes seen in Fig. 9(a).

[1] T. J. Kippenberg, H. Rokhsari, T. Carmon, A. Scherer, and K. J. Vahala, Phys. Rev. Lett. **95**, 033901 (2005).

[2] O. Arcizet, P.-F. Cohadon, T. Briant, M. Pinard, and A. Heidmann, Nature (London) **444**, 71 (2006).

[3] S. Gigan, H. R. Böhm, M. Paternostro, F. Blaser, G. Langer, J. B. Hertzberg, K. C. Schwab, D. Bäuerle, M. Aspelmeyer, and A. Zeilinger, Nature (London) **444**, 67 (2006).

[4] T. J. Kippenberg and K. J. Vahala, Science **321**, 1172 (2008).

[5] F. Marquardt and S. M. Girvin, Physics **2**, 40 (2009).

[6] O. Romero-Isart, A. C. Pflanzer, M. L. Juan, R. Quidant, N. Kiesel, M. Aspelmeyer, and J. I. Cirac, Phys. Rev. A **83**, 013803 (2011).

[7] O. Romero-Isart, Mathieu L. Juan, Romain Quidant, and J. I. Cirac, New J. Phys. **12**, 033105 (2010).

[8] O. Romero-Isart, A. C. Pflanzer, F. Blaser, R. Kaltenbaek, N. Kiesel, M. Aspelmeyer, and J. I. Cirac, Phys. Rev. Lett. **107**, 020405 (2011).

[9] D. E. Chang, K.-K. Ni, O. Painter, and H. J. Kimble, New J. Phys. **14**, 045002 (2012).

[10] D. E. Chang *et al.*, Proc. Natl. Acad. Sci. USA **107**, 1005 (2010).

[11] T. Corbitt, Y. Chen, E. Innerhofer, H. Muller-Ebhardt, D. Ottaway, H. Rehbein, D. Sigg, S. Whitcomb, C. Wipf, and N. Mavalvala, Phys. Rev. Lett. **98**, 150802 (2007).

[12] A. Schliesser, P. Del'Haye, N. Nooshi, K. J. Vahala, and T. J. Kippenberg, Phys. Rev. Lett. **97**, 243905 (2006).

[13] M. Eichenfield, C. P. Michail, R. Perahia, and O. Painter, Nature Photon. **1**, 416 (2007).

[14] S. Gröblacher, K. Hammerer, M. R Vanner, and M. Aspelmeyer, Nature (London) **460**, 724 (2009).

[15] M. L. Gorodetksy, A. Schliesser, G. Anetsberger, S. Deleglise, and T. J. Kippenberg, Opt. Express **18**, 23236 (2010).

[16] J. D. Thompson *et al.*, Nature (London) **452**, 72 (2008).

[17] E. Verhagen, S. Delglise, S. Weis, A. Schliesser, and T. J. Kippenberg, Nature (London) **482**, 63 (2012).

[18] F. Marquardt, J. P. Chen, A. A. Clerk, and S. M. Girvin, Phys. Rev. Lett. **99**, 093902 (2007).

[19] I. Wilson-Rae, N. Nooshi, W. Zwerger, and T. J. Kippenberg, Phys. Rev. Lett. **99**, 093901 (2007).

[20] C. Genes, D. Vitali, P. Tombesi, S. Gigan, and M. Aspelmeyer, Phys. Rev. A **77**, 033804 (2008).

[21] A. D. O Connell *et al.*, Nature (London) **464**, 08967 (2010).

[22] R. Riviere, S. Deleglise, S. Weis, E. Gavartin, O. Arcizet, A. Schliesser, and T. J. Kippenberg, Phys. Rev. A **83**, 063835 (2011).

[23] J. D. Teufel, T. Donner, Dale Li, J. W. Harlow, M. S. Allman, K. Cicak, A. J. Sirois, J. D. Whittaker, K. W. Lehnert, and R. W. Simmonds, Nature (London) **475**, 359 (2011).

[24] J. Chan, T. P. Mayer Alegre, A. H. Safavi-Naeini, J. T. Hill, A. Krause, S. Gröblacher, M. Aspelmeyer, and O. Painter, Nature (London) **478**, 89 (2011).

[25] M. Aspelmeyer *et al.*, J. Opt. Soc. Am. B **27**, A189 (2010).

[26] S. Basiri-Esfahani, U. Akram, and G. J. Milburn, New J. Phys. **14**, 085017 (2012).

[27] M. Ludwig, A. H. Safavi-Naeini, O. Painter, and F. Marquardt, Phys. Rev. Lett. **109**, 063601 (2012).

[28] A. H. Safavi-Naeini and O. Painter, New J. Phys. **13**, 013017 (2011).

[29] K. Stannigel, P. Komar, S. J. M. Habraken, S. D. Bennett, M. D. Lukin, P. Zoller, and P. Rabl, Phys. Rev. Lett. **109**, 013603 (2012).

[30] H. Muller-Ebhardt, H. Rehbein, R. Schnabel, K. Danzmann, and Y. Chen, Phys. Rev. Lett. **100**, 013601 (2008).

[31] M. J. Hartmann and M. B. Plenio, Phys. Rev. Lett. **101**, 200503 (2008).

[32] D. Vitali, S. Mancini, and P. Tombesi, J. Phys. A **40**, 8055 (2007).

[33] D. Vitali, S. Gigan, A. Ferreira, H. R. Bohm, P. Tombesi, A. Guerreiro, V. Vedral, A. Zeilinger, and M. Aspelmeyer, Phys. Rev. Lett. **98**, 030405 (2007).

[34] C. Wipf *et al.*, New J. Phys. **10**, 095017 (2008).

[35] L. Mazzola and M. Paternostro, Phys. Rev. A **83**, 062335 (2011).

[36] G. Heinrich, M. Ludwig, J. Qian, B. Kubala, and F. Marquardt, Phys. Rev. Lett. **107**, 043603 (2011).

[37] G. Heinrich and F. Marquardt, Europhys. Lett. **93**, 18003 (2011).

[38] K. Stannigel, P. Rabl, and P. Zoller, New J. Phys. **14**, 063014 (2012).

[39] C. Joshi, J. Larson, M. Jonson, E. Andersson, and P. Öhberg, Phys. Rev. A **85**, 033805 (2012)

[40] H. J. Carmichael, Phys. Rev. Lett. **70**, 2273 (1993).

[41] C. W. Gardiner, Phys. Rev. Lett. **70**, 2269 (1993).

[42] C. W. Gardiner and P. Zoller, *Quantum Noise* (Springer, Berlin, 2004).

[43] G. Vidal and R. F. Werner, Phys. Rev. A **65**, 032314 (2002).

[44] C. Genes, A. Mari, D. Vitali, and P. Tombesi, Adv. At. Mol. Opt. Phys. **57**, 33 (2009).

[45] J. Eisert, M. B. Plenio, S. Bose, and J. Hartley, Phys. Rev. Lett. **93**, 190402 (2004).